ACS OMEGA

http://pubs.acs.org/journal/acsodf

Article

# Slurryability and Influencing Mechanism of Hydrophobic Structures in Additive−Coal−Water Ternary System

Wenjing Zhang, Shichao Li,* Ruizhi Chu,* Shaolian Ma, Weisong Li, Yulong Li, Tonghua Zhang, Xianliang Meng, and Jianqiao Zhao

Cite This: *ACS Omega* 2022, 7, 10167−10177

Read Online

ACCESS | Metrics & More | Article Recommendations

**ABSTRACT:** This study investigates the effects of additive adsorption onto coal particles on surface properties, hydrophobic groups on the slurryability, and the moisture occurrence form on the performance of coal water slurry (CWS). Mechanisms related to the different hydrophobic structures of the additives are proposed. The adsorption method of sulfonated acetone formaldehyde enhances the adsorption capacity of coal surfaces but is not conducive to slurrying. Sodium lignin sulfonate has hydrophobic ends with nonpolar aromatic groups, three-dimensional macromolecular structures, and complex branched chains, which provide CWS with good stability and slurryability. Naphthalenesulfonate formaldehyde has a double benzene ring structure and provides the thick but nonuniform adsorption layers on coal surfaces. The many amorphous structures and low molecular weights of sodium humic sulfonate lead to nonuniform hydration films and poor slurryability. The results of this paper provide guidance for improving synergism in coal−water−additive systems and enhancing slurry performance.

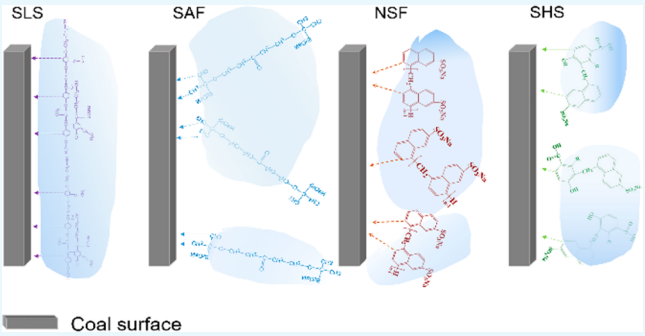


## 1. INTRODUCTION

Coal is one of the most important fossil fuels in the world. In recent years, the demand for fossil fuel energy has increased.[1] Coal water slurry (CWS) is composed of approximately 60−75% coal, 25−40% water, and 1% additives; it is environmentally friendly and has high combustion efficiency.[2] A high-quality CWS should exhibit a high solid content and low viscosity; the additives used are vitally important in this regard.[3] At present, the anionic additives used in industrial applications include naphthalenesulfonates, aliphatic sulfonates, lignin sulfonates, humate sulfonates, and carboxylate.[4−7]

The properties of CWS are influenced by the physical and chemical properties of the coal surfaces, such as their oxygen-containing functional groups, electric charges, hydrophilicity, inherent moisture, and pore structure.[8,9] Additives are reversely adsorbed on coal surfaces because of the presence of oxygen-containing functional groups. This results in nonuniform adsorption of additives on the coal surfaces, which influences slurry performance.[10,11] Electrostatic repulsion is provided by the charges on the coal surfaces, which disperses the coal particles and improves the stability of the slurry.[12,13] The nonuniformity of coal surface structures is not beneficial to slurryability; therefore, additives are used in CWS to improve this situation. The hydrophobic structure of the additives is adsorbed onto coal surfaces and links to the water molecules through the hydrophilic end, which makes the wettability of the coal surfaces more uniform. In addition, the ionization of additives in water can introduce more charges on the coal surfaces and further improve the dispersion performance of the slurry.[14−16]

Mohanta et al. revealed that lignin sulfonate (LS) provides a greater adsorption capacity to coal surfaces than oxidized sulfomethylated lignin (OSL), with the introduction of repulsion between suspended particles making the CWS more stable.[17] Wang et al. showed that the viscosity of CWS is sensitive to alkali additives and increases with additive content. When the concentration of the alkaline solution is low, the zeta-potential of the particles in CWS decreases and the free water content increases.[18] Mukherjee et al. measured contact angles and zeta-potentials to investigate the magnitude of interface energy. They found that the hydrophobic/hydrophilic forces between coal particles are greater than those of electrostatic forces. They established a model based on a modified Krieger−Dougherty (K−D) equation to predict slurry viscosity.[19] Xia et al. investigated the hydrophobic

Received: November 15, 2021
Accepted: March 2, 2022
Published: March 14, 2022





https://doi.org/10.1021/acsomega.1c06431
*ACS Omega* 2022, 7, 10167−10177

Table 1. Proximate and Ultimate Sample Analyses

| proximate analysis (wt %) | | | | ultimate analysis (wt %) | | | | |
|---|---|---|---|---|---|---|---|---|
| $M_{ad}$ | $A_d$ | $V_{daf}$ | $FC_{daf}$ | $C_{daf}$ | $H_{daf}$ | $O_{daf}$ | $N_{daf}$ | $S_{vd}$ |
| 6.73 | 8.95 | 35.59 | 64.41 | 76.30 | 4.23 | 18.14 | 0.71 | 0.62 |

mechanism of dodecyl trimethylammonium bromide (DTAB) on low-rank coal surfaces and found that electrostatic forces play an important role in the adsorption of DTAB onto low-rank coal surfaces.[20] Lu et al. established a coal−water interface model to analyze the diffusion mechanism of naphthalenesulfonate formaldehyde (NSF) in CWS. They found that the form of moisture occurrence changed from a bound state to a free state, thereby improving the hydrophobicity of the coal surfaces.[21]

The factors affecting the performance of CWS are complex. Most researchers have focused on the effect of a single component (additive structure or coal structure) on the performance of CWS and have ignored the synergism among these three aspects. In this study, the ability of anionic additives to modify coal surfaces was investigated based on their adsorption behavior. This revealed the influences of different additives on Shenhua coal. The forms of slurry moisture occurrence were inferred from the characteristics of slurry moisture evaporation. This research aimed to explain the CWS formation mechanism from the perspective of changes in the physical and chemical properties of the coal surfaces and the synergism of the additives−coal−water system.

## 2. EXPERIMENTAL METHODS

**2.1. Materials.** Shenhua noncaking coal from Inner Mongolia, China, was selected for the experiment. The results of proximate and ultimate analyses are listed in Table 1. The raw coal was dried and then milled by a sealed prototype machine (KER-FK100A, Kerui Sample Preparation Equipment Co., Ltd., China). It was then coarsely sieved into particles <2 mm in diameter and dried at 25 °C for 24 h in air. The coal powder is sealed and stored for subsequent experiments. The particle size distribution of the resulting coal powder is presented in Figure 1.

Additives of NSF were synthesized through sulfonation, hydrolysis, condensation, and neutralization reactions. The naphthalene in NSF as a hydrophobic group and the sulfonic acid group as a hydrophilic group played a role in slurrying. The sulfonated acetone formaldehyde (SAF) was synthesized using carbonyl groups as raw materials and introducing sulfonic acid groups as hydrophilic groups. The sodium lignin sulfonate (SLS) was obtained by modifying lignin; SLS has nonpolar groups such as alkylbenzene but also has sulfonic acid groups, methoxy groups, hydroxyl groups, and other polar groups. The aromatic ring in sodium humic sulfonate (SHS) is hydrophobic, and the sulfonic acid groups and hydroxyl groups connected to the ring are hydrophilic.

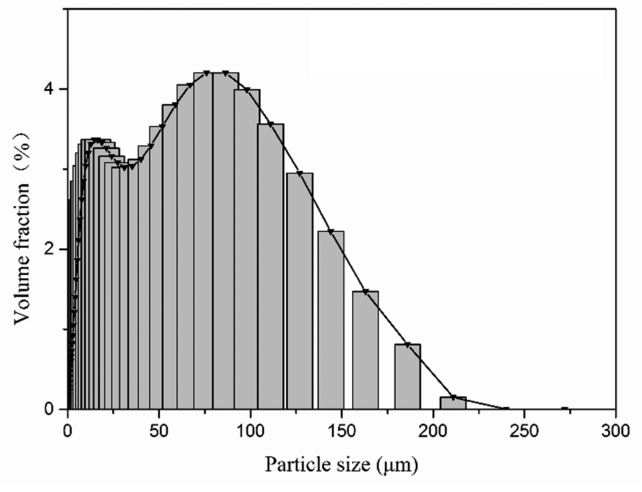


Figure 1. Particle size distribution of a coal sample.

**2.2. Preparation of CWS.** Dry slurrying was adopted in the experiment. The 100 g pulverized coal (dry basis) and the additives weighed proportionally were added into a beaker; deionized water was then added several times in small amounts and stirred with a glass rod until the slurry was formed. Then the mixture was stirred at 1500 rpm for 15 min to form CWS.[22]

**2.3. Adsorption Experiment.** *2.3.1. Adsorption Measurement.* A total of 0.5 g coal (previously milled), 50 mL of deionized water, and additive solutions of different concentrations were added into a conical flask. The solution was shaken in a water bath oscillator (SHA-CA, Jintan Youlian Equipment and Instrument Research Institute, China, ± 0.5 °C) at 30 °C at a shaking frequency of 170 rpm for 7 h. The mixture was left standing for 24 h and then the supernatant was taken for centrifugation for 15 min; finally, the supernatant after centrifugation was taken to measure the absorbance. An ultraviolet spectrophotometer (UV-1600, Shanghai Reunion Scientific Instrument Co., Ltd., China, ±2 nm) was used to measure the absorbance of the supernatant. The saturated adsorption capacity of the additives on the coal particle surfaces was calculated using the following formula:

$$Q_e = \frac{(C_0 - C_e)V}{m} \quad (1)$$

where $Q_e$ (mg/g) is the saturation adsorption capacity; $C_0$ (mg/L) is the initial concentration of the additive solution; $C_e$ (mg/L) is the concentration of additive solution at adsorption equilibrium; $V$ (L) is the volume of solution; each set of samples is 50 mL; and $m$ (g) is the weight of the coal sample, which is 0.5 g.

*2.3.2. Adsorption Fitting and Free Energy.* Langmuir and Freundlich models were used to fit curves of the adsorption characteristics of the additives on the coal surface.

(1) Langmuir isothermal adsorption equation

$$Q_e = \frac{K_L Q^m C^e}{1 + K_L C_e} \quad (2)$$

$$\frac{1}{Q_e} = \frac{1}{K_L Q_m} \cdot \frac{1}{C_e} + \frac{1}{Q_m} \quad (3)$$

where $Q_e$ (mg/g) is the equilibrium adsorption capacity; $C_e$ (mg/L) is the solution concentration at adsorption equilibrium; $Q_m$ (mg/g) is the saturation adsorption; and $K_L$ is the Langmuir constant.

(2) Freundlich isothermal adsorption equation



https://doi.org/10.1021/acsomega.1c06431
ACS Omega 2022, 7, 10167−10177

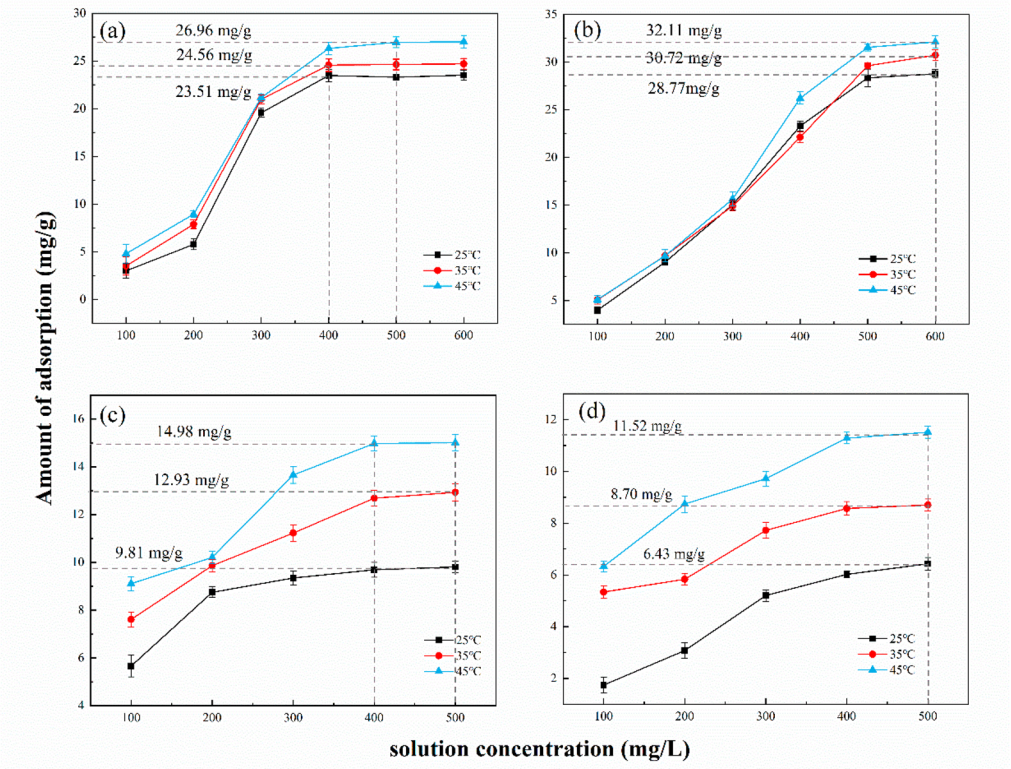


**Figure 2.** Adsorption isotherm curves of coal samples with (a) SAF, (b) NSF, (c) SLS, and (d) SHS additives. Error bars are ± confidence intervals for the three sets of data at $P$ = 95%.

$$Q_e = K_F \cdot C_e^{1/n} \tag{4}$$

$$\ln Q_e = \frac{1}{n} \ln C_e + \ln K_F \tag{5}$$

where $Q_e$ (mg/g) is the equilibrium adsorption capacity; $C_e$ (mg/L) is the solution concentration at adsorption equilibrium; $K_F$ (mg/g) is the adsorption capacity; and $n$ is the Freundlich constant.

The free energy of adsorption $\Delta G_0$ can be calculated by formula 6:[23]

$$\Delta G_0 = -RT \ln K_0 \tag{6}$$

$$K_0 = 1000 K_L M_A \tag{7}$$

where $R$ is the ideal gas constant; $T$ (K) is the absolute temperature; $K_0$ is the equilibrium constant; $K_L$ is the Langmuir constant; $M_A$ (g/mol) is the molecular weight of adsorbate; and $\Delta G_0$ (kJ/mol) is the adsorption free energy.

**2.4. Analysis of Coal Surface Properties.** *2.4.1. Contact Angle Measurement.* The contact angle of water on the coal surfaces (of raw coal and coal with dispersant) was measured with a contact angle meter (JC2000D1, Shanghai Zhongchen Digital Technology Equipment Co., Ltd., China, ±1°).

*2.4.2. Zeta-Potential Measurement.* A microelectrophoresis instrument (JS94G, Shanghai Zhongchen Digital Technology Equipment Co., Ltd., China, system error <5%) is used to measure the zeta-potentials of the samples. A total of 0.5 g of slurry particles was dissolved in 50 mL of distilled water, and the adsorption reached equilibrium after standing for 24 h. The zeta-potential of the supernatant was measured, and a slurry without additives was used as a control.

*2.4.3. Surface Energy Analysis of Coal.* The surface energy was calculated by the Owens two-liquid method. The contact angle of the liquid (water and *n*-hexadecane) on coal surfaces was measured. The surface energy was calculated as follows:[24]

$$\gamma_{L_1}(1 + \cos\theta_1) = 2(\gamma_s^D \gamma_{L_1})^{1/2} + 2(\gamma_s^D \gamma_{L_1}^P)^{1/2} \tag{8}$$

$$\gamma_{L_2}(1 + \cos\theta_2) = 2(\gamma_s^D \gamma_{L_2})^{1/2} + 2(\gamma_s^P \gamma_{L_2}^P)^{1/2} \tag{9}$$

$$\gamma_s = \gamma_s^D + \gamma_s^P \tag{10}$$

where $\gamma_s$ is the solid surface energy; $\gamma_L$ is the liquid surface energy; $\gamma_s^D$ is the dispersion force; $\gamma_s^P$ is the polar force; and $\theta$ is the contact angle between the liquid and coal surface.

**2.5. Slurry Measurement.** *2.5.1. Slurry Properties.* The viscosity of CWS was determined by a rotary viscometer (NXS-4C, Chengdu Instrument Factory, China, ±5%) at shear rates of 10, 20, 40, 60, 80, and 100 $s^{-1}$. The relationship between the shear stress and shear rate of CWS was fitted using the three-parameter Herschel–Bulkley model (formula 11), which can be used to judge the slurry flow model.[25] By putting a certain volume of CWS ($V_2$) into a test tube and recording the volume of supernatant ($V_1$) after 7 days, the water bled rates can be obtained.

$$\tau = \tau_0 + K\dot{\gamma}^n \tag{11}$$

where $\tau$ (Pa) is the shear stress; $\tau_0$ (Pa) is yield stress; $\dot{\gamma}$ ($s^{-1}$) is the shear rate; and $K$ is the consistency coefficient. The Herschel–Bulkley model can represent common fluid flow patterns such as Newtonian fluids, pseudoplastic fluids, dilatant fluids, Bingham plastic fluids, etc. The slurry flow pattern can be judged by the $n$ value. When the rheological index $n$ is equal to 1, the fluid is Newtonian fluid; when $n$ is less than 1, the fluid is pseudoplastic fluid; and when $n$ is greater than 1, the fluid is a dilatant fluid.



https://doi.org/10.1021/acsomega.1c06431
ACS Omega 2022, 7, 10167−10177

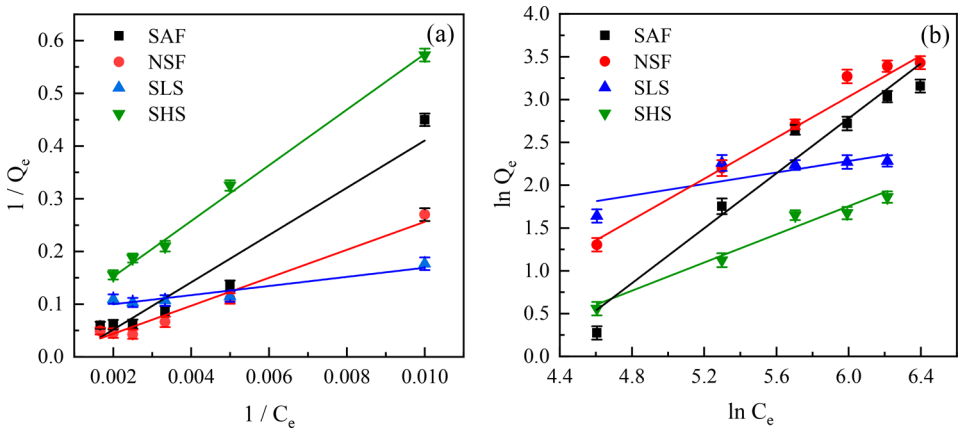


**Figure 3.** Fitting curves of the adsorption of additives on the coal surface with different equation at 25 °C: (a) Langmuir and (b) Freundlich). Error bars are ± confidence intervals for the three sets of data at $P$ = 95%.

*2.5.2. Water Content Measurement.* The thermal weight loss of the slurry was measured by a simultaneous thermal analyzer (NETZSCH 409C, Germany, ±0.1 °C). A moisture evaporation curve was obtained by increasing the slurry temperature from 25 to 130 °C at a rate of 5 °C/min. The moisture evaporation rate was obtained according to differential derivation of the evaporation curve.

*2.5.3. Adsorption Layer Thickness Measurement.* The adsorption layer thickness of the additives was measured through X-ray photoelectron spectroscopy (XPS) (Escalab 250Xi, USA).[26,27] The $Si_{2p}$ element existed in the coal but not in the additives; therefore, it was used as the characteristic element to calculate the adsorption layer thickness of the additives on the coal surface. The photoelectron strength of $Si_{2p}$ should decrease after additive is adsorbed on coal particles. The adsorption layer thickness was obtained by calculating the change in the $Si_{2p}$ photoelectron peak area (eq 12):[28]

$$d = -\ln(I_d/I_0) \times \lambda(E_k) \quad (12)$$

where $I_0$ is the incident photoelectron intensity; $d$ (nm) is the thickness of the adsorptive film; and $I_d$ is the photoelectron intensity passing through the adsorption layer.

$$\lambda(E_k) = 49E_k^{-2} + 0.11(E_k)^{1/2} \quad (13)$$

where $\lambda$ ($E_k$) is the average depth of photoelectron escape (nm) and $E_k$ (eV) is the photoelectron kinetic energy.

$$E_k = h\nu - E_b \quad (14)$$

where $h$ is the Planck constant; $\nu$ is the photoelectron rate; and $E_b$ (eV) is the atomic binding energy.

*2.5.4. Microscopic Aggregation Morphology of Slurry.* The particle distribution of CWS was observed by microscope (Nikon E100, Japan). A certain amount of slurry was smeared on glass slides; then after being air-dried, the sample was observed under a microscope at 1000× magnification.

## 3. RESULTS AND DISCUSSION

**3.1. Adsorption Process Analysis.** The adsorption quantity of additives on the coal surface was determined by the isothermal adsorption experiment. Figure 2 shows that, within a certain temperature range, increasing the temperature is conductive to the adsorption of the four additives on the coal surface. As the molecular structure of the additives was large, heating was conducive to stretching of the molecular structure and increasing its solubility, thereby increasing the amount of additive adsorbed on the coal surfaces. As can be seen from Figure 2c,d, the adsorption of SLS and SHS is more susceptible to temperature. As the molecular structure of SLS and SHS is relatively complex, they are natural macromolecular compound. When the temperature increased substantially, the hydrophobic end was exposed to improve the adsorption capacity. Lignin is derived from plant cellulose, and the molecular weight of lignin is larger than that of humic acid. This result proves that the molecular structure of the hydrophobic end of SHS is smaller than that of the SLS, resulting in lesser adsorption capacity. The adsorption capacity finally tended to the equilibrium with the increase of additive

**Table 2. Fitting Parameters of the Isotherm Adsorption Equation of Coal Samples with Different Additives**

| | Langmuir | | | Freundlich | | |
|---|---|---|---|---|---|---|
| additive | $Q_m$ | $K_L$ | $R^2$ | $n$ | $K_F$ | $R^2$ |
| SAF | 35.33 | 0.0087 | 0.896 | 0.6208 | 0.0010 | 0.976 |
| NSF | 23.25 | 0.0985 | 0.993 | 0.8340 | 0.0155 | 0.987 |
| SLS | 11.05 | 1.0050 | 0.989 | 2.9654 | 1.3003 | 0.862 |
| SHS | 6.90 | 0.0012 | 0.990 | 1.2116 | 0.0400 | 0.971 |

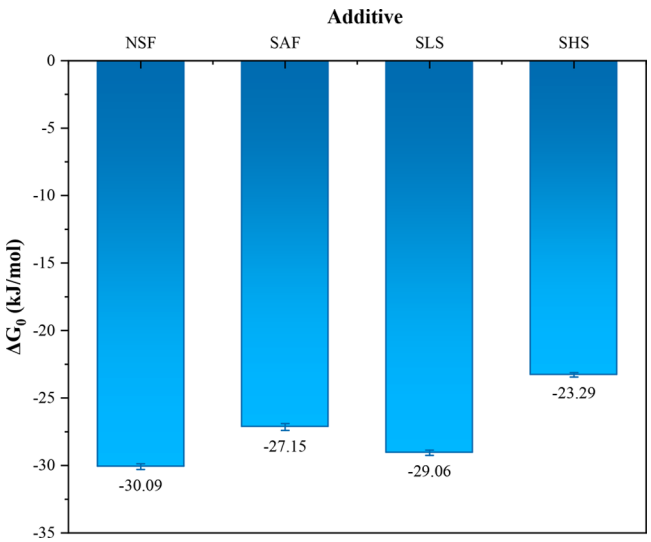


**Figure 4.** Adsorption free energies of different additives. Error bars are ± confidence intervals for the three sets of data at $P$ = 95%.



https://doi.org/10.1021/acsomega.1c06431
ACS Omega 2022, 7, 10167−10177

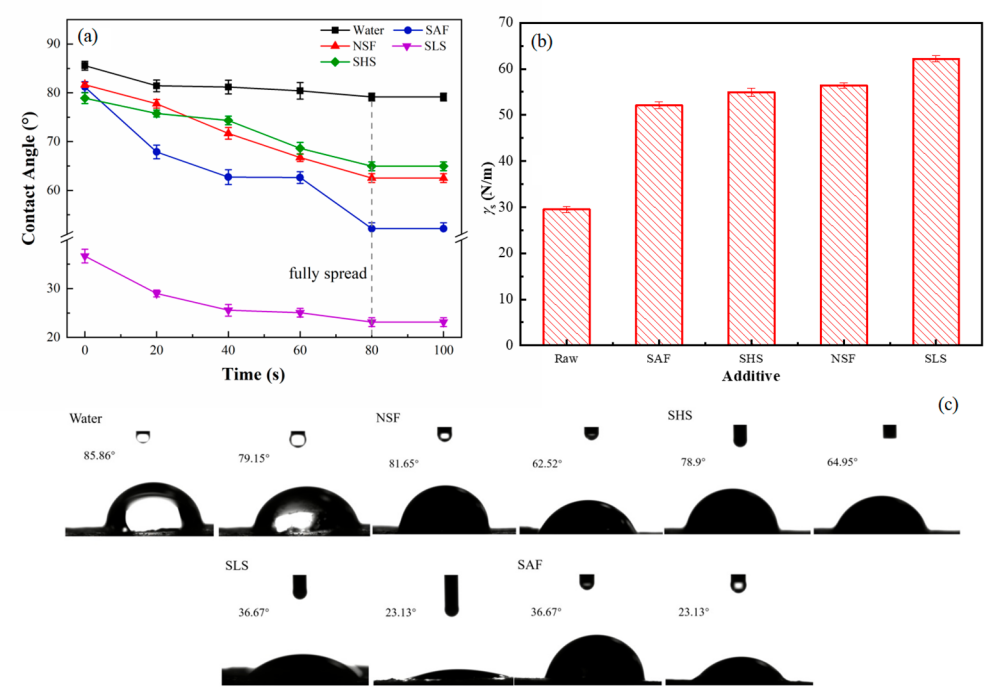


**Figure 5.** Physicochemical properties of coal surfaces: (a) graphs of variation in these contact angles with time, (b) surface energies of coal surfaces modified by the different additives, and (c) images of contact angles of additive solution before and after being completely spread on the coal surface. Error bars are ± confidence intervals for the three sets of data at $P$ = 95%.

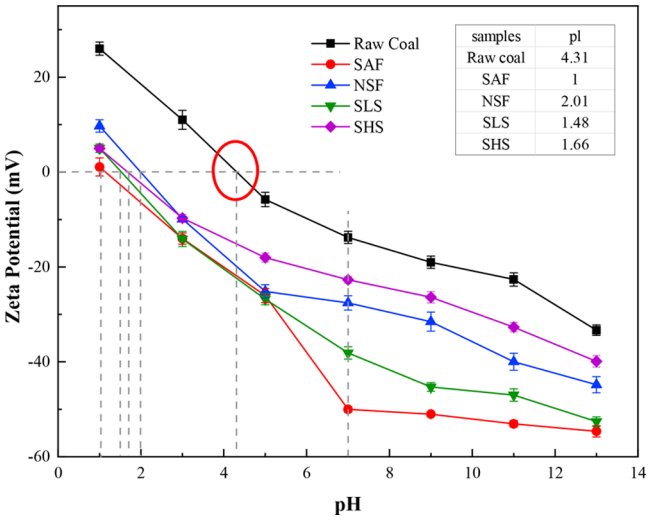


**Figure 6.** Zeta-potentials of coal particles with different additives adsorbed on their surfaces. Error bars are ± confidence intervals for the three sets of data at $P$ = 95%.

concentration, and the maximum equilibrium adsorption capacity of NSF reached 32.11 mg/g.

The results of adsorption curve fitting are shown in Figure 3 and Table 2. The adsorption behavior of NSF, SLS, and SHS is more consistent with the Langmuir adsorption model; therefore, these three additives are indicative of monolayer adsorption, and monolayer adsorption can reduce the probability of cross-linking among molecules, which is conducive to the improvement of adsorption efficiency. While the adsorption behavior of SAF is more consistent with the Freundlich model. This indicates that the adsorption sites on the coal surface are selective for SAF, and this adsorption may be chemical adsorption. At the same time, SAF has a complex long-chain structure, and cross-linking may occur between molecules. Therefore, the adsorption of SAF on the coal surface is not uniform.

The adsorption free energies of different additives were calculated by the thermodynamic formulas 6 and 7. Figure 4 shows that the adsorption free energy of the additives on coal surfaces was <0. This indicates that the additive adsorption process can occur spontaneously. NSF was adsorbed on the coal surface in a monolayer with the maximum absolute value of adsorption free energy of −30.09 kJ/mol, hence, adsorption between its hydrophobic ends and coal surfaces was easier; this is because the NSF additive has a double benzene ring structure similar to that of the condensed aromatic rings of coal's molecular structure and polarity—similar adsorbates and adsorbents increase NSF adsorbed on coal surfaces. The adsorption amount of SLS on the coal surface was small, and the absolute value of the adsorption free energy was large. SLS was a long-chain structure containing aromatic rings; therefore, SLS may be adsorbed on the coal surface uniformly in a horizontal type. There were more polar structures in the SHS molecules and a few polar oxygen functional groups on the coal surfaces. Hence, the interaction between polar functional groups caused an antiadsorption phenomenon, which is unfavorable to the slurrying process. It is found that the adsorption behavior of SAF was more in line with the Freundlich adsorption model from the Table 2. This may be due to the long-chain structure of SAF. When the hydrophobic end was adsorbed on the coal surface, the molecular chain might be twisted, and cross-links would occur between the molecules. Therefore, the adsorption of SAF on the coal surface adsorption sites is not uniform and irregular.

### 3.2. Physicochemical Properties of the Coal Surfaces.

The effects of the additives on the physicochemical properties of the coal surfaces were studied in terms of contact angle, surface energy, and zeta-potential. As shown in Figure 5a,c, the



https://doi.org/10.1021/acsomega.1c06431
ACS Omega 2022, 7, 10167−10177

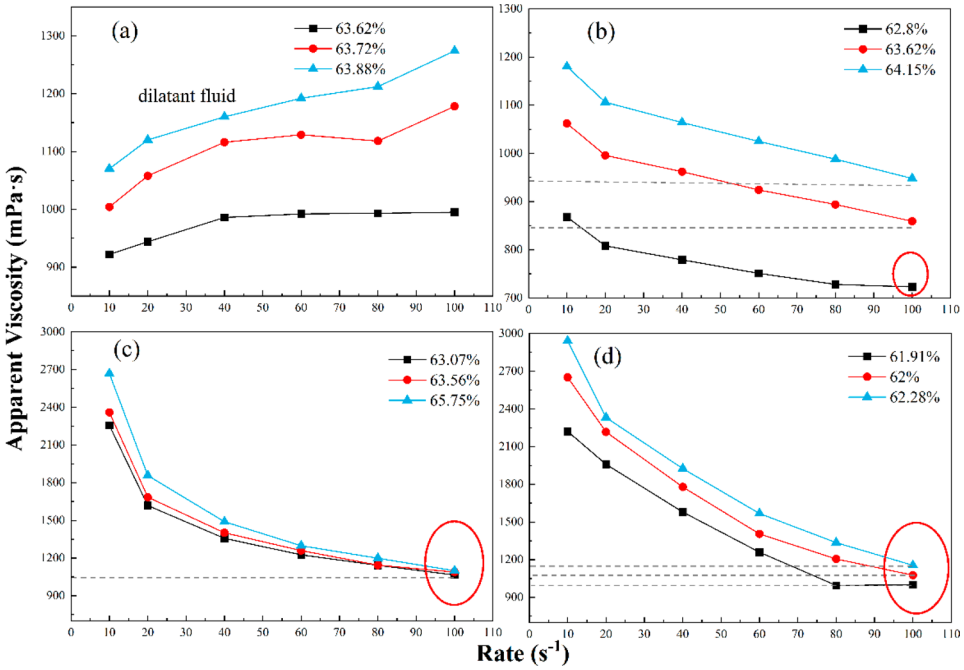


**Figure 7.** Apparent viscosities of CWS with different additives: (a) SAF, (b) NSF, (c) SLS, and (d) SHS.

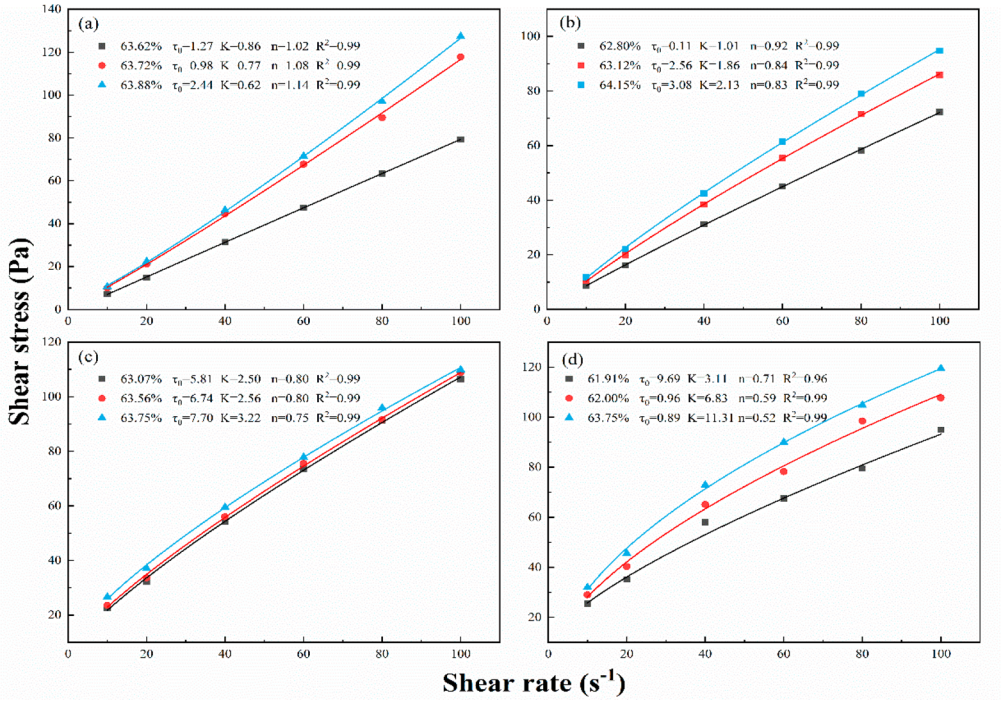


**Figure 8.** Shear stress curves of slurries with different additives: (a) SAF, (b) NSF, (c) SLS, and (d) SHS.

contact angle of the coal−water interface reflected the wettability of the coal surface. The smaller the contact angle, the better the hydrophilicity of the coal. At 80 s, the water was completely spread out on the coal surface adsorbed with the four additives. The contact angle of the coal surface that adsorbed with SAF changed the most before and after spreading, hence, it has strong spreading ability and permeability on the coal surface. The contact angle of the coal surface adsorbed by SLS was significantly smaller than that of other additives, indicating that SLS had the best effect on improving the wettability of the coal surface. The contact angle of coal surface that adsorbed with SHS is larger than that after adsorption of other additives, indicating that the improvement effect of SHS on the wettability of the coal surface is poor. There were more oxygen functional groups and fewer aromatic structures on the SHS molecules than the other additives. Therefore, the interaction strength between the additive molecules and coal surface was not uniform (strong at the polar site of the coal and weak at the water level), which had an adverse effect on the spreading ability. The contact angle, spreading ability, and permeability of the additives are related to their properties and interactions with the coal surface.



https://doi.org/10.1021/acsomega.1c06431
ACS Omega 2022, 7, 10167−10177

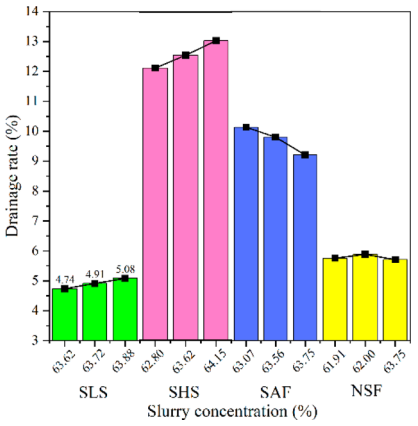


**Figure 9.** Water bled rates of CWS with different additives.

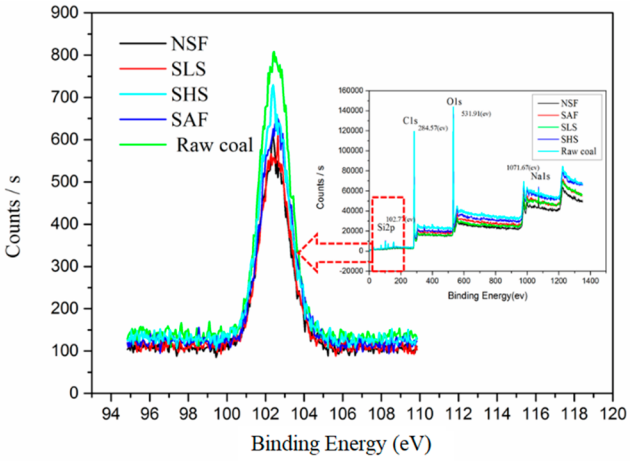


**Figure 11.** XPS spectra of different slurry particles.

Hence, the slurryability of the additives needs to be further explored by experiments.

Figure 5b shows that the modified coal surfaces were obviously improved compared with raw coal. The surface energy of the SLS-modified coal surfaces reached 62.2 N/m, which is why it had the smallest contact angle on the coal surface. The SLS additive can provide a large number of hydrophilic sites because it contained many polar functional groups (hydroxyl, carboxyl, carbonyl, etc.). Although the contact angle of the NSF additive solution is greater than that of SAF, the NSF-modified coal surface energy is 56.4 N/m, indicating that the interaction strength was large between NSF and the coal surface, and its modification effect is fine. Differences in coal surface energy are the result of the additives having different molecular structures and interaction strengths with the coal surfaces. The influences of the additives on the wettability of coal surfaces can be determined by surface energy measurements.

Figure 6 shows that the isoelectric point of raw coal is 4.31. The pH corresponding to the isoelectric point decreased after adding additives. SAF had the largest adsorption capacity and more charge, causing the pH value to decrease the most. The zeta value of SLS was lower than those of NSF and SHS as it contained more polar groups and ionized in water. There were more polar bridge bonds (−C−O; −O−) in SHS molecules than in others, so the ionization effect of SHS molecules was affected by intermolecular cross-linking.

**3.3. Analysis of Slurry Performance.** The percentages in Figure 7 are the concentrations of the CWS made in three parallel experiments, that is, the mass percentage of solids (coal and additives) in the slurry. As shown in Figure 7a, the SAF additive caused the slurry to exhibit the properties of a dilatant

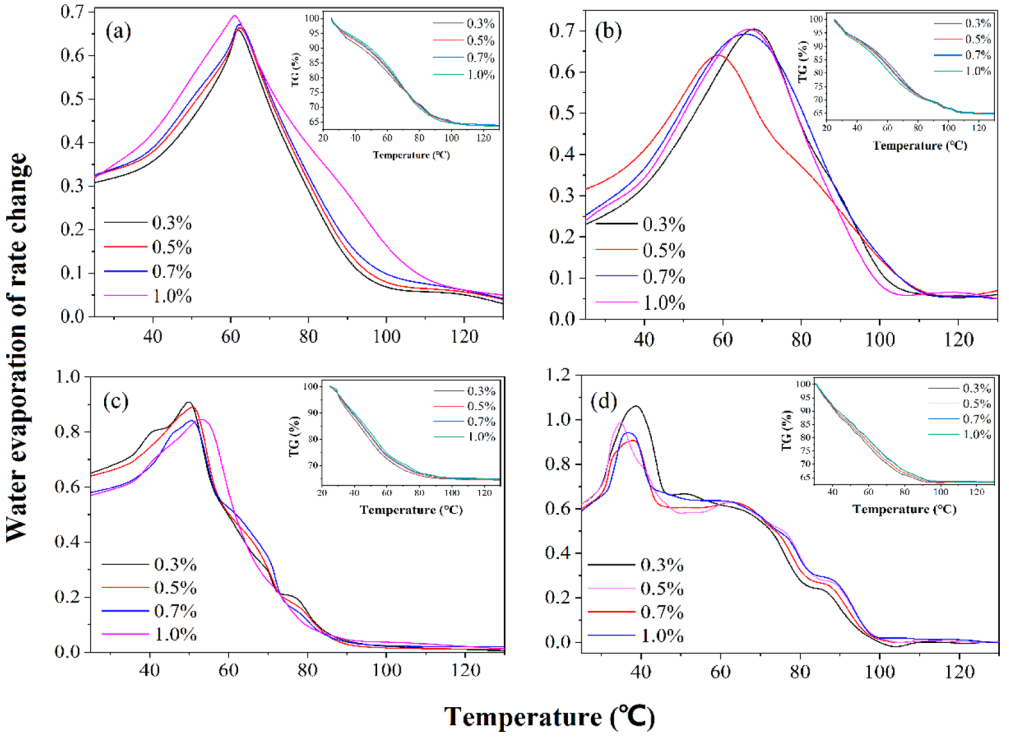


**Figure 10.** Variations in the water evaporation rates of slurries containing different amounts of additives: (a) SAF, (b) NSF, (c) SLS, and (d) SHS.



https://doi.org/10.1021/acsomega.1c06431
ACS Omega 2022, 7, 10167−10177

Table 3. Adsorption Layer Thicknesses of Different Additives

| sample | peak (eV) | area (P) CPS (eV) | atomic % | $\lambda$ ($E_k$) | $-\ln(I_d/I_0)$ | thickness (nm) |
|---|---|---|---|---|---|---|
| raw coal | 102.89 | 42,083.21 | 6.28 | | | |
| NSF | 102.69 | 16,105.70 | 5.23 | 1.119 | 0.960 | 1.313 |
| SAF | 102.87 | 18,366.05 | 4.17 | 1.120 | 0.829 | 1.167 |
| SLS | 102.83 | 17,842.28 | 4.56 | 1.120 | 0.858 | 1.199 |
| SHS | 102.77 | 25,795.59 | 4.34 | 1.119 | 0.489 | 0.786 |

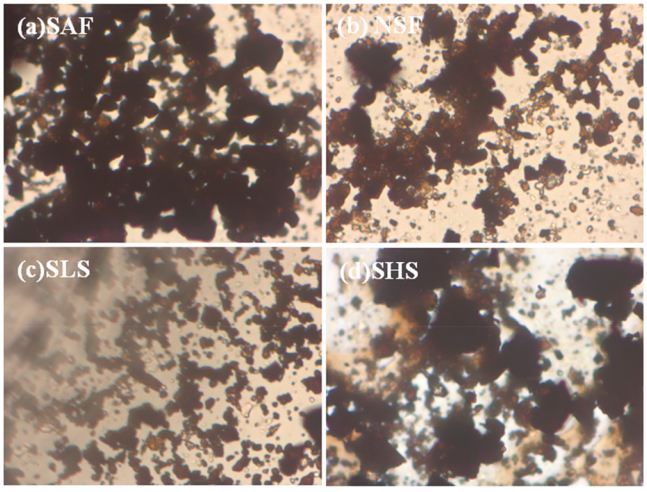


**Figure 12.** Microscopic aggregation states of slurry systems containing (a) SAF, (b) NSF, (c) SLS, and (d) SHS.

fluid, which is contrary to the CWS's requirement of shear thinning. Figure 7b–d shows that the slurries containing NSF, SLS, and SHS additives exhibited pseudoplastic fluid properties. SLS was adsorbed on the coal surfaces, and the sulfonate acted as bridges connecting the hydrophilic ends and water molecules to form a stable hydration film. This hydration film can reduce friction among coal particles, thereby reducing the viscosity of the slurry. NSF formed a hydration film because it contains double benzene rings linked to the coal surface. In contrast, SHS has an amorphous structural unit and cannot form a uniform hydration film, so the CWS with SHS had the highest apparent viscosity.

The percentages in Figures 8 and 9 are the concentrations of the CWS made in three parallel experiments, that is, the mass percentage of solids (coal and additives) in the slurry. It can be seen from Figures 8 and 9 that the $n$ value of SAF is greater than 1, which indicates that the slurry belongs to expansive plastic fluid. This result is consistent with the phenomenon of "shear thickening" shown by the apparent viscosity of SAF. SAF could not meet the slurryability requirements. This indicates that the adsorption form of SAF on coal surfaces is not conducive to slurry formation, and the slurry has a high water bled rate. The $n$ value of the slurry prepared by the other three dispersants is less than 1, indicating that they all show the property of shear thinning, which are consistent with the results of viscosity curves. The yield stress $\tau_0$ of NSF is smaller than that of SLS and SHS, indicating that NSF has better fluidity and can easily overcome resistance to make the slurry flow. The water bled rate of NSF was about 5%, and it had an obvious shear thinning property. Its apparent viscosity meets the industrial application requirements with a viscosity of 1000–1200 mPa·s at a shear rate of 100/$s^{-1}$. The SLS additive exhibited good slurryability and showed obvious shear thinning property. The $K$ value of the SLS system was larger than that of the NSF system, so it was characterized by a "thick" property. The SLS slurry had the highest slurry concentration. More water molecules were adsorbed due to the presence of polar functional groups, which led to a lower water bled rate and higher stability. The SHS additive has a low molecular weight that does not match that of the coal, resulting in a poor slurrying effect.

The percentages in Figure 10 refer to different amounts of additives. It can be seen from Figure 10 that the water variations trend for the same additive under different addition amounts are consistent. Therefore, the influence of different additives on the water occurrence form can be analyzed through the experimental results. Some of the water molecules in CWS are free-flowing (free water), whereas the others are bounded by the polar and spatial structures of the additives (bound water). Figure 10b,c shows that the NSF and SLS slurries were more difficult to dehydrate because their water evaporation rates were lower than those of the other two cases. The variations in water evaporation rates presented in Figure 10d showed that the water volatilization process of the second stage was longer than that in the SHS slurry systems. As this additive contains more polar functional groups, the proportions of bound water molecules in their slurry systems were higher. The moisture distribution proportion of SLS and NSF was better, and the inflection point of the evaporation rate curve appeared later. There was only a small time difference between the two processes of water evaporation, so the distribution of water proportions in the NSF and SLS slurry was more uniform. Hydration films were formed on the coal surfaces in the slurry system, and there was enough free water to make the slurry have good fluidity and stability.

As shown in Figure 11, the elemental silicon on the coal surfaces was covered by the adsorption layer formed by the additives, which caused the photoelectron strength to decrease significantly. The NSF additive has a naphthalene ring structure, while the main structural molecular units of coal are naphthalene and anthracene rings. Therefore, the molecular interaction between NSF and coal was strong and the thickness of the adsorption layer reached 1.31 nm (Table 3). Due to its horizontal adsorption method, the adsorption layer thickness of SLS was larger than that of SHS. However, the long-chain molecular structure of SLS made its adsorption layer thinner than that of NSF with a double benzene ring structure. SHS have more branched-chain structures with hydroxyl, carboxyl and other functional groups, which hinder their adsorption processes and cause their adsorption layers to be thinner than that of NSF. Isothermal adsorption experiments showed that the adsorption method of SAF on the coal surfaces is unfavorable to the formation of a stable and thick adsorption layer during the adsorption process.

Microscopic aggregation in slurry systems containing different additives was observed by microscope (Figure 12). SLS provided the best dispersion of coal particles, which is why the SLS slurry had the best stability. The zeta-potential


https://doi.org/10.1021/acsomega.1c06431
ACS Omega 2022, 7, 10167–10177

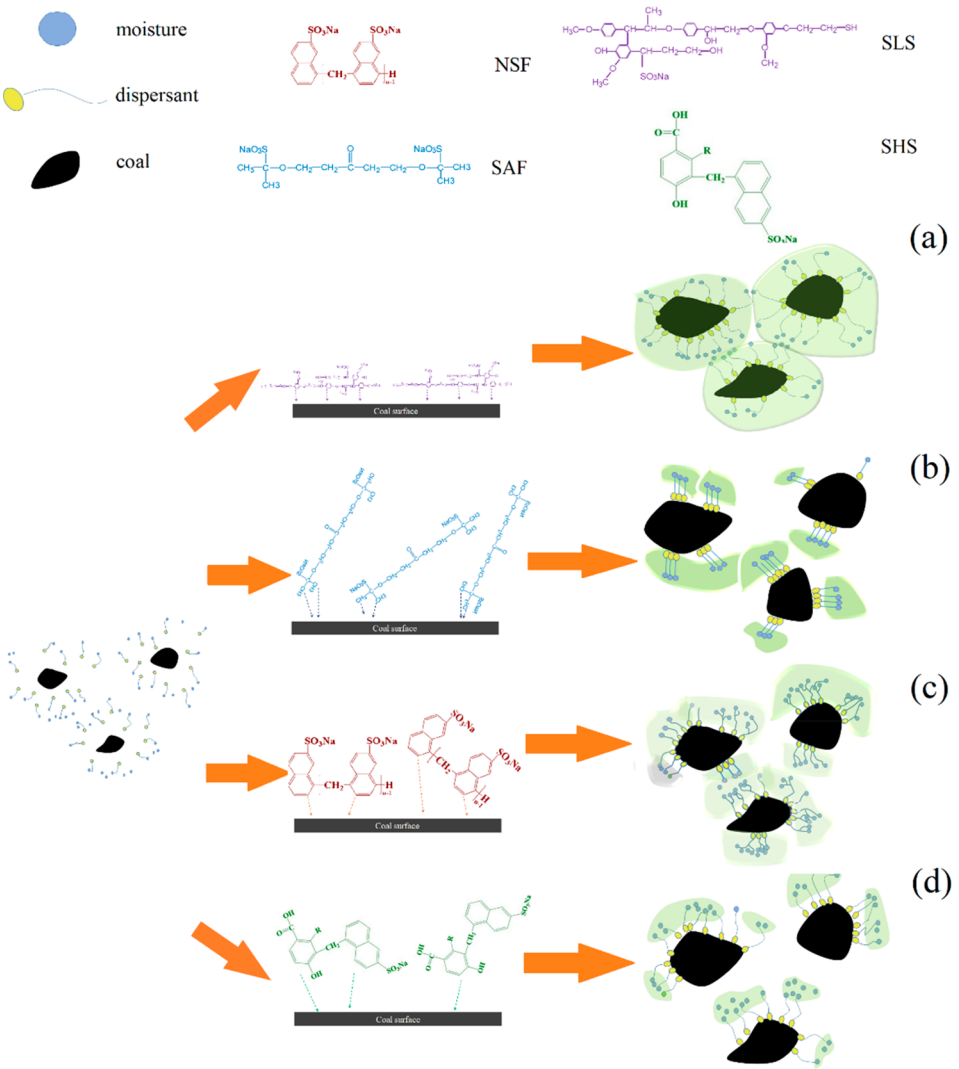


**Figure 13.** Synergistic slurrying mechanisms of additive−coal−water ternary systems containing (a) SLS, (b) SAF, (c) NSF, and (d) SHS.

measurements show that the SAF additive increases the absolute zeta-potential on the coal surfaces. However, the dispersion effects of the NSF and SLS additives were better than that of SAF. Therefore, the dispersion of additives is the result of multiple factors, and the adsorption mode of SAF was unfavorable to slurry formation. Additives build bridges between coal and water by adsorption on the coal surfaces. The original coal−water interfacial structure is destroyed, and coal particles wrapped in hydration film resist sedimentation. This further improves the dispersion effect, reduces friction between coal particles, and improves flow performance.

**3.4. Slurrying Mechanisms in Additive−Coal−Water Ternary Systems.** Nonuniform distributions of additives result in incomplete hydration films forming on coal surfaces. This study found that the SLS additive has a unique adsorption mode and can form stable and uniform distributions on coal surfaces to form the slurry system shown in Figure 13a. The adsorption density of SAF on the coal surfaces was nonuniform, as shown in Figure 13b. NSF can form the hydration films due to the double benzene structure, but the hydration film formed is thicker than that of SLS (Figure 13c). The SHS additive has a light molecular weight and many polar groups, giving it less effective adsorption on coal surfaces and poorer hydration films (Figure 13d). In the slurry system, some of the water formed hydration films on coal surfaces, which is conducive to the uniform dispersion of slurry particles and improves slurry stability. Part of the water was in a free state, which can improve the fluidity of slurry when it flows. Therefore, an appropriate water distribution is favorable to coal−water−additive synergism.

## 4. CONCLUSION

The effects of different hydrophobic structures on the formation of hydration films were studied from the perspective of synergism in additive−water−coal ternary systems. A mechanism by which hydrophobic structures influence slurrying was proposed. SAF has a nonuniform adsorption density and forms poor hydration films on the surfaces of Shenhua coal particles, resulting in poor slurrying. When the SLS additive was added to the system, the slurry showed the best stability, and the improvement of the wettability of the coal surface and the particle dispersion effect of SLS was better than that of the other three additives. The strength of the interaction between NSF additive and coal surfaces is enhanced by NSF's naphthalene ring structure, resulting in the thickest adsorption layers of up to 1.31 nm. However, the modification effect of NSF on the wettability and zeta-potential of coal is worse than that of SLS, and the dispersion effect of



https://doi.org/10.1021/acsomega.1c06431
ACS Omega 2022, 7, 10167−10177

coal particles is also worse than that of SLS. Due to the light molecular weights and many amorphous structures of SHS, the hydration films it forms on coal surfaces are ineffective, and the adsorption capacity is the lowest. The SHS molecules are difficult to match with the coal types; therefore, the slurryability is poor. This paper provides guidance for the use of anionic additives in CWS. Certain specific issues warrant further study, such as the influence of adsorption film thickness on slurry performance.

## AUTHOR INFORMATION


### Corresponding Authors

**Shichao Li** − *Faculty of Materials and Chemical Engineering, Yibin University, Yibin 644000, China*; Email: mysimpledesign@163.com

**Ruizhi Chu** − *School of Chemical Engineering and Technology, China University of Mining & Technology, Xuzhou 221116, China*; orcid.org/0000-0003-4712-6906; Email: 4038@cumt.edu.cn

### Authors

**Wenjing Zhang** − *School of Chemical Engineering and Technology, China University of Mining & Technology, Xuzhou 221116, China*

**Shaolian Ma** − *School of Chemical and Environmental Engineering, North China Institute of Science and Technology, Langfang, Hebei 065201, China*

**Weisong Li** − *School of Chemical Engineering and Technology, China University of Mining & Technology, Xuzhou 221116, China*

**Yulong Li** − *School of Chemical Engineering and Technology, China University of Mining & Technology, Xuzhou 221116, China*

**Tonghua Zhang** − *School of Chemical Engineering and Technology, China University of Mining & Technology, Xuzhou 221116, China*

**Xianliang Meng** − *School of Chemical Engineering and Technology, China University of Mining & Technology, Xuzhou 221116, China*

**Jianqiao Zhao** − *School of Chemical Engineering and Technology, China University of Mining & Technology, Xuzhou 221116, China*

Complete contact information is available at: https://pubs.acs.org/10.1021/acsomega.1c06431


### Notes

The authors declare no competing financial interest.

## ACKNOWLEDGMENTS

This work was supported by the National Natural Science Foundation of China (Grant Nos. 51974308 and 51974312), National Key R&D Program of China (Grant No. 2019YFE0100100), Major Science and Technology Project of Shanxi Province (Grant No. 20181102017), and Postgraduate Research & Practice Innovation Program of Jiangsu Province (KYCX21_2308).

## REFERENCES


(1) Nunes, L. J. R. Potential of Coal−Water Slurries as an Alternative Fuel Source during the Transition Period for the Decarbonization of Energy Production: A Review. *Appl. Sci.* **2020**, *10*, 2470.

(2) Khanpit, V.; Tajane, S. P.; Mandavgane, S. A. Experimental studies on coal-water slurry fuel prepared from pretreated low-grade coal. *Int. J. Coal Prep. Util* **2019**, *1*−*15*, 1.

(3) Hu, S.; Liu, L.; Yang, X.; Li, J.; Zhou, B.; Wu, C.; Weng, L.; Liu, K. Influence of different dispersants on rheological behaviors of coal water slurry prepared from a low quality coal. *RSC. Adv.* **2019**, *9*, 32911−32921.

(4) Du, L.; Zhang, G. H.; Yang, D. D.; Luo, J.; Liu, Y. W.; Zhang, W. B.; Zhang, C.; Li, J. G.; Zhu, J. F. Synthesis of a novel amphoteric copolymer and its application as a dispersant for coal water slurry preparation. *R. Soc. Open. Sci.* **2021**, *8*, 201480.

(5) Savitskii, D. P.; Dimitryuk, T. N.; Makarov, A. S. Sedimentation of coal particles in lower aliphatic alcohols and the stability of alcohol-coal suspensions. *Solid Fuel Chem.* **2016**, *50*, 39−45.

(6) Yan, M.; Yang, D. Adsorption Mechanism of Lignosulfonate at the Air/Liquid Interface. *J. Brazil. Chem. Soc.* **2015**, *26*, 555−61.

(7) Zhang, W. B.; Luo, J.; Huang, Y.; Zhang, C.; Du, L.; Guo, J.; Wu, J.; Zhang, X.; Zhu, J. F.; Zhang, G. H. Synthesis of a novel dispersant with topological structure by using humic acid as raw material and its application in coal water slurry preparation. *Fuel* **2020**, *262*, 116576.

(8) Yu, J. D.; Jiang, C. Y.; Guan, Q. Q.; Gu, J. J.; Ning, P.; Miao, R. G.; Chen, Q. L.; Zhang, J. M. Conversion of low-grade coals in sub- and supercritical water: A review. *Fuel* **2018**, *217*, 275−84.

(9) Yu, J. L.; Tahmasebi, A.; Han, Y. N.; Yin, F. K.; Li, X. C. A review on water in low rank coals: The existence, interaction with coal structure and effects on coal utilization. *Fuel Process. Technol.* **2013**, *106*, 9−20.

(10) Chu, R. Z.; Li, Y. L.; Meng, X. L.; Fan, L. L.; Wu, G. G.; Li, X.; Jiang, X. F.; Yu, S.; Hu, Y. F. Research on the slurrying performance of coal and alkali-modified sludge. *Fuel* **2021**, *294*, 120548.

(11) Meng, Z. Y.; Yang, Z. Y.; Yin, Z. Q.; Li, Y. Y.; Ju, X. Q.; Yao, Y. Q.; Long, J. Interaction between dispersant and coal slime added in semi-coke water slurry: An experimental and DFT study. *Appl. Surf. Sci.* **2021**, *540*, 148327.

(12) Li, L.; Ma, C. D.; Lin, M. Y.; Liu, M. P.; Yu, H.; Wang, Q. B.; Cao, X. Q.; You, X. F. Study of sodium lignosulfonate prepare low-rank coal-water slurry: Experiments and simulations. *Chin. J. Chem. Eng.* **2021**, *29*, 344−53.

(13) Chen, J.; Min, F. F.; Liu, L. Y.; Peng, C. L.; Lu, F. Q. Hydrophobic aggregation of fine particles in high muddied coal slurry water. *Water Sci. Technol.* **2016**, *73*, 501−10.

(14) Xin, F. D.; Xu, H.; Tang, D. Z.; Yang, J. S.; Chen, Y. P.; Cao, L. K.; Qu, H. X. Pore structure evolution of low-rank coal in China. *Int. J. Coal Geol* **2019**, *205*, 126−39.

(15) Xu, C. H.; Wang, D. M.; Wang, H. T.; Ma, L. Y.; Zhu, X. L.; Zhu, Y. F.; Zhang, Y.; Liu, F. M. Experimental investigation of coal dust wetting ability of anionic surfactants with different structures. *Process Saf. Environ* **2019**, *121*, 69−76.

(16) Rao, Z. H.; Zhao, Y. M.; Huang, C. L.; Duan, C. L.; He, J. F. Recent developments in drying and dewatering for low rank coals. *Prog. Energy Combust* **2015**, *46*, 1−11.

(17) Mohanta, S. K.; Rath, S. S.; Dwari, R. K. Surface functionalization of coal and quartz with aniline: A study on work function and frictional charge. *Powder Technol.* **2018**, *338*, 233−42.

(18) Wang, C. Y.; Zhao, H.; Dai, Z. H.; Li, W. F.; Liu, H. F. Influence of alkaline additive on viscosity of coal water slurry. *Fuel* **2019**, *235*, 639−46.

(19) Mukherjee, A.; Pisupati, S. V. Interparticle Interactions in Highly Concentrated Coal−Water Slurries and Their Effect on Slurry Viscosity. *Energy Fuel* **2015**, *29*, 3675−83.

(20) Xia, Y. C.; Yang, Z. L.; Zhang, R.; Xing, Y. W.; Gui, X. H. Enhancement of the surface hydrophobicity of low-rank coal by adsorbing DTAB: An experimental and molecular dynamics simulation study. *Fuel* **2019**, *239*, 145−52.

(21) Lu, H. Y.; Li, X. F.; Zhang, C. Q.; Chen, J. Y.; Ma, L. G.; Li, W. H.; Xu, D. P. Experiments and molecular dynamics simulations on the adsorption of naphthalenesulfonic formaldehyde condensates at the coal-water interface. *Fuel* **2020**, *264*, 116838.

(22) Li, D.; Liu, J.; Wang, S.; Cheng, J. Study on coal water slurries prepared from coal chemical wastewater and their industrial application. *Appl. Energ* **2020**, *268*, 114976.
(23) Mukherjee, A.; Pisupati, S. V. Effect of additives on interfacial interactions for viscosity reduction of carbonaceous solid-water slurries. *Fuel* **2016**, *180*, 50−8.
(24) Bechikh, A.; Klinkova, O.; Maalej, Y.; Tawfiq, I.; Nasri, R. Sandblasting parameter variation effect on galvanized steel surface chemical composition, roughness and free energy. *Int. J. Adhes. Adhes* **2020**, *102*, 102653.
(25) Li, P. W.; Yang, D. J.; Qiu, X. Q.; Feng, W. S. Study on Enhancing the Slurry Performance of Coal−Water Slurry Prepared with Low-Rank Coal. *J. Disper. Sci. Technol.* **2015**, *36*, 1247−56.
(26) Singh, J.; Mukherjee, A.; Sengupta, S. K.; Im, J.; Peterson, G. W.; Whitten, J. E. Sulfur dioxide and nitrogen dioxide adsorption on zinc oxide and zirconium hydroxide nanoparticles and the effect on photoluminescence. *Appl. Surf. Sci.* **2012**, *258*, 5778−5785.
(27) Zhang, K.; Ma, J. Z.; Lyu, B.; Shi, G. X.; Zhou, B.; Tian, Y. Influence of "tentacle structure" on the properties of jellyfish-like 3D dispersants based on tannic acid for preparing high-concentrated coal−water slurry. *Fuel* **2020**, *274*, 117860.
(28) Zhu, J. F.; Wang, P.; Li, Y. B.; Li, J. G.; Zhang, G. G. Dispersion performance and mechanism of polycarboxylates bearing side chains of moderate length in coal-water slurries. *Fuel* **2017**, *190*, 221−8.



https://doi.org/10.1021/acsomega.1c06431
*ACS Omega* 2022, 7, 10167−10177